Regular Article

PHYSICAL CHEMISTRY RESEARCH
Published by the
Iranian Chemical Society
www.physchemres.org
info@physchemres.org

Phys. Chem. Res., Vol. 6, No. 3, 547-563, September 2018
DOI: 10.22036/pcr.2018.128713.1481

DFT Study on Oxygen-Vacancy Stability in Rutile/Anatase TiO_2: Effect of Cationic Substitutions

S.M. Esfandfard[a], M.R. Elahifard[b,c,*], R. Behjatmanesh-Ardakanii[a] and H. Kargar[a]

[a]*Department of Chemistry, Payame Noor University, P. O. Box: 19395-3697 Tehran, Iran*
[b]*Chemical Engineering Department, Faculty of Engineering, Ardakan University, Iran*
[c]*Ayatollah Khatami Boulevard, P. O. Box: 184, Ardakan University, Ardakan, Iran*

(Received 26 April 2018, Accepted 18 May 2018)

In this study, a full-potential density functional theory was used to investigate the effects of Ti substitution by different cations. In both rutile and anatase, Ti atom was replaced by Ce, Au, Sn, Ag, Mo, Nb, Zr and Y. Phase stability, electronic structure and formation energy of oxygen vacancy were compared for rutile and anatase. The results indicated that substitution of Ce and Zr increases anatase stability through which photocatalytic activity is enhanced. It seems that the cationic capacity and size play a critical role in anatase to rutile phase transition, where with an equi- or higher valence than Ti, larger cations increase the stability of anatase phase. Oxygen vacancy concentration, as a second factor of photocatalytic activity, was also studied by calculating its stability due to the cationic substitution. The data revealed that Au, Ag, Y, Ce and Sn effectively reduce oxygen-vacancy formation energy. Of the studied cations, Au and Ag had maximum reduction in band gap, by creating defect states in the middle of the band gap resulting from the overlaps of d-orbitals of these elements and oxygen p-orbitals. Mo and Ce impurities did not have a significant effect on reducing gaps by creating defect states under the conduction band. Finally, Sn impurity also generated defect states in the middle of the gap merely with the lack of oxygen.

Keywords: TiO_2-based photocatalysts, Anatase and rutile, Oxygen deficiency, Full-potential density functional theory

INTRODUCTION

Titanium dioxide (titania) has attracted a great deal of attention in different industrial fields such as renewable energy, self-cleaning, and pollutant removal due to its low price, amphoteric nature, and biocompatibility [1-8]. Owing to the energy levels of valence and conduction bands and their capacity, titania is introduced as a high-performance photocatalyst, capable of producing hydrogen out of water splitting process (solar hydrogen) and oxidizing different organic molecules in response to sunlight [9-14]. As with other semi-conductor photocatalysts, titania facilitates reactions from production of electron-hole pairs (e-h) through radiation beyond semiconductor energy gap.

Titania has two main phases, rutile phase which is stable thermodynamically, and anatase phase which is pseudo-stable and converted to rutile by increasing heat [15,16]. Previous studies have revealed that anatase is a better photocatalyst than rutile due to its indirect band gap (low e-h recombination) and higher specific surface area [17-19]. However, its main deficiency is high band gap (3.2 eV) which covers only a small region of sunlight [20-22]. Two main approaches for this problem involve increasing O-vacancy concentration and/or substituting Ti by other cations [23-35]. O-vacancy and Ti-substitution introduce band gap engineering by locating some new bands in the forbidden region of the band gap [36-40]. Both processes bring about the following effects: the band gap declines; charge separation and thus e-h recombination rate medium gap state; the oxygen vacancies react in the reaction as active surface centers [41,42].

Experiments have shown that anatse to rutile can be

*Corresponding author. E-mail: mrelahifard@ardakan.ac.ir

prevented through substitution of cations with a high charge density [43-47]. However, this is not a general rule, and a cation with a high charge density can enhance anatase to rutile phase transformation. Therefore, the details of mechanism of reducing or enhancing anatse to rutile phase transformation are open challenging questions [48].

Generally, doping and oxygen vacancy both can affect the crystalline and electronic structures and in turn the system performance [49,50]. Two electrons leaving from O-vacancy can occupy Ti levels whose energy reduction is associated with decreased conduction band energy. On the other hand, use of action in substitutional or interstitial form introduces a new band in the band gap region.

In this work, 4d cations with large cationic radius size including Y, Zr, Nb, Mo and Ag have been considered to study the effect of cation substitution and O-vacancy, simultaneously, on the anatse to rutile phase transition. Further, substitution of Au atom on which various experimental studies have been conducted was added to this list. Recently, a group of researchers have investigated anatase to rutile transformation experimentally, and examined its importance in the presence of Sn and Ce impurity. Thus, in this work, to confirm theoretical calculations with experimental data, these impurities were also considered.

The paper is organized as follows: in the next section, details of computation are discussed, then the results and analysis of geometry optimization calculations are presented along with relative energy of anatase and rutile, formation energy of oxygen vacancy defect and electronic structure (*i.e.* band structure, density of states (DOS) and partial DOS (pDOS)) for anatase and rutile pure structures and also for doped with cations, with and without oxygen vacancy defects. .

CALCULATION DETAILS

ZORA approach has been considered to increase correctness of calculations. The criteria for convergence of energy, density and force were set to 5×10^{-6} eV, 5×10^{-5} eV and 0.2 eV/Å, respectively [54]. $4 \times 4 \times 6$ and $6 \times 6 \times 2$ k-grids have been used to model the first brillouin zone for rutile and anatase unit cells, respectively. $2 \times 2 \times 1$ and $2 \times 2 \times 2$ supercells for anatase and rutile have been used to study effect of doped cations (Fig. 1). Rutile and anatase supercells contain 48 atoms which are 12Ti + 36O. The concentration of cations is equal to 6.25% at. Also, in all calculations, O-vacancy concentration was set to be 3.125% at. (only one oxygen atom has been removed from the supercell). Then, concurrent with dopants and oxygen defect, by investigating all different states, we found the most stable site for developing oxygen defect in the anatase and rutile structures in the presence of impurity. Figure 2 reveals the most stable form.

In this paper, we have studied the effect of O-vacancy and dopant on the model, simultaneously. To study the effects of O-vacancy and dopant, pDOS and band structure of all supercells have been calculated. For band structure, Γ (0.0 0.00.0) - X (0.0 0.5 0.5) - Γ - Z (0.5 0.5 -0.5) - N (0.0 0.5 0.0) - P (0.25 0.25 0.25) - Z - X - P directions have been considered. k-gird for all DOS calculations was set to $12 \times 12 \times 27$ and $27 \times 27 \times 12$ for rutile and anatse, respectively.

RESULTS AND DISCUSSION

Unit Cell

Experimental cell parameters for rutile (r-TiO_2) are a = 4.594 Å and c = 2.959 Å and for anatase (a-TiO_2), these parameters are a = 3.784 Å, c = 9.514 Å [55]. Our pbe calculation results for rutile were a = 4.57 Å and c = 2.94 Å, and for anatase were a = 3.75 Å and c = 9.6 Å. After structural relaxation, electronic properties of anatase and rutile phase of titania were analyzed. Figure 3 illustrates DOS and band structure in which anatase and rutile phases had a band gap energy of 2.1 and 1.8 eV. These values are lower than the experimental values (3 and 3.2 eV for anatase and rutile, respectively) which are due to intrinsic limitation of DFT calculations. However, DFT calculations can precisely predict the relative energy gap which was the aim of this study as well. Also, pDOS calculation analysis indicated that for both anatase and rutile phases, oxygen p-orbitals and titanium d-orbitals have a major contribution to the upper edge of the valence band and the lower edge of the conduction band, respectively (Fig. 4).

In this work, ΔE was defined as E(r-TiO_2) - E(a-TiO_2), representing the extent of phase stability in TiO_2. Positive ΔE suggests that energetically, a-TiO_2 is more desirable than r-TiO_2. DFT calculations indicated that a-TiO_2 is more

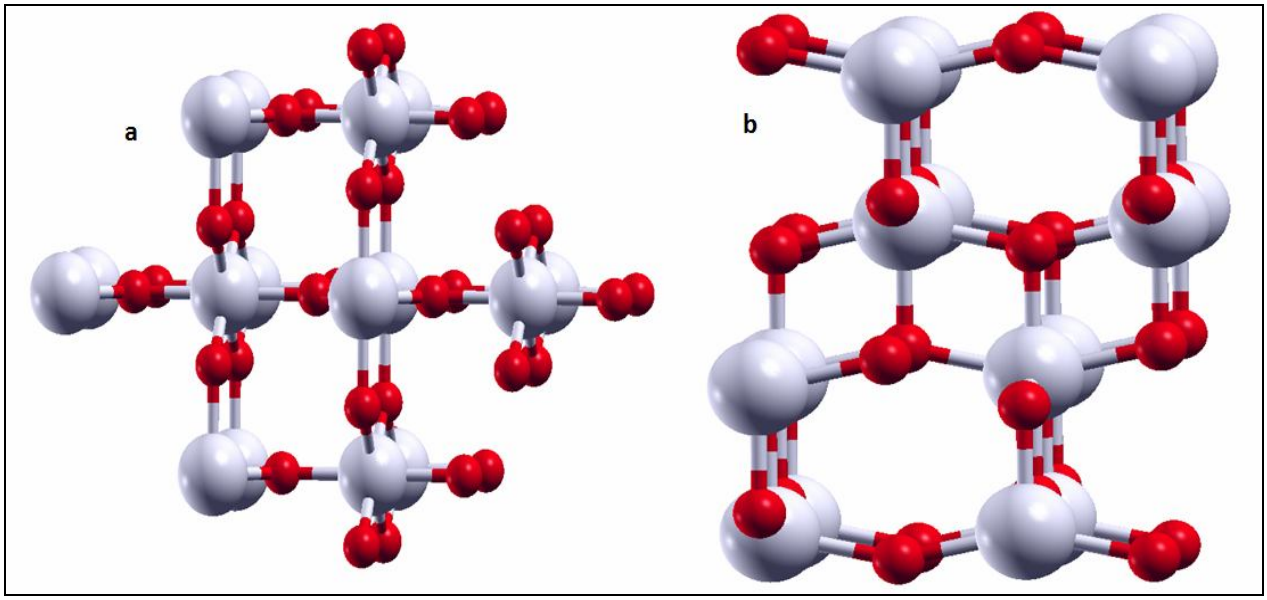

Fig. 1. The crystalline structure of the computational model of 2 × 2 × 2 and 2 × 2 × 1, 48-atom supercell for rutile (a) and anatase (b), titanium atoms are represented by light grey circles, while oxygen atoms are demonstrated by red circles.

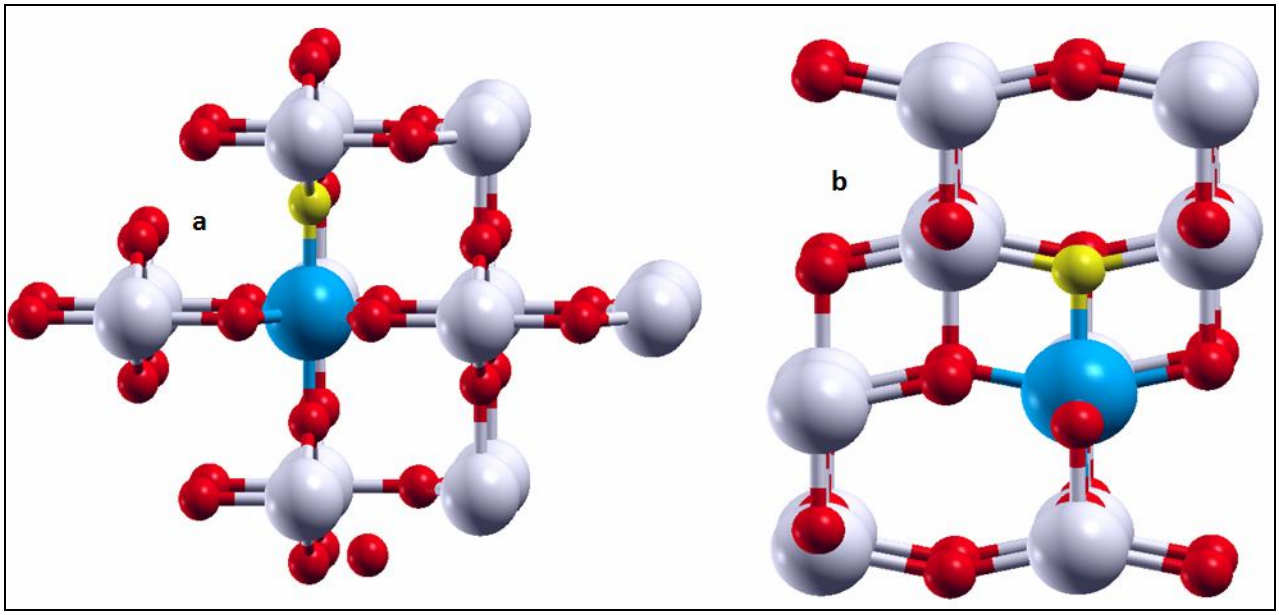

Fig. 2. The crystalline structure of the computational model of 2 × 2 × 2 and 2 × 2 × 1, 48-atom supercell doped with transition metal impurity along with oxygen vacancy for rutile (a) and anatase (b). Titanium, impurity and oxygen atoms are shown by light grey, blue and red circles, respectively. The oxygen vacancy position has been represented by the yellow circle.

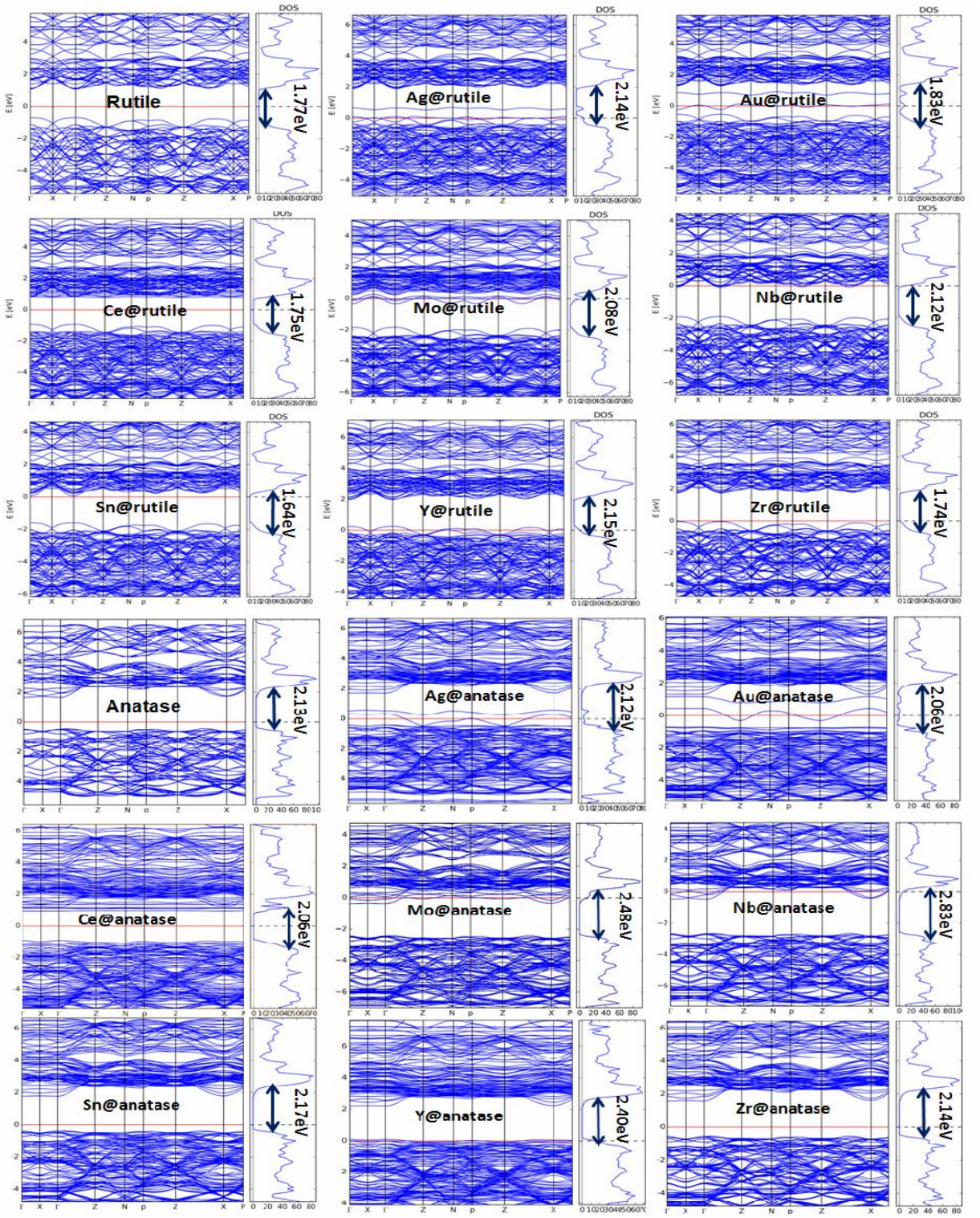

Fig 3. The total DOS and band structure of doped anatase and rutile TiO_2 compare with Pure TiO_2. Red solid line represents of the Fermi level. The band gap values were determined from Γ point, where the defect sates inside the gap were ignored.

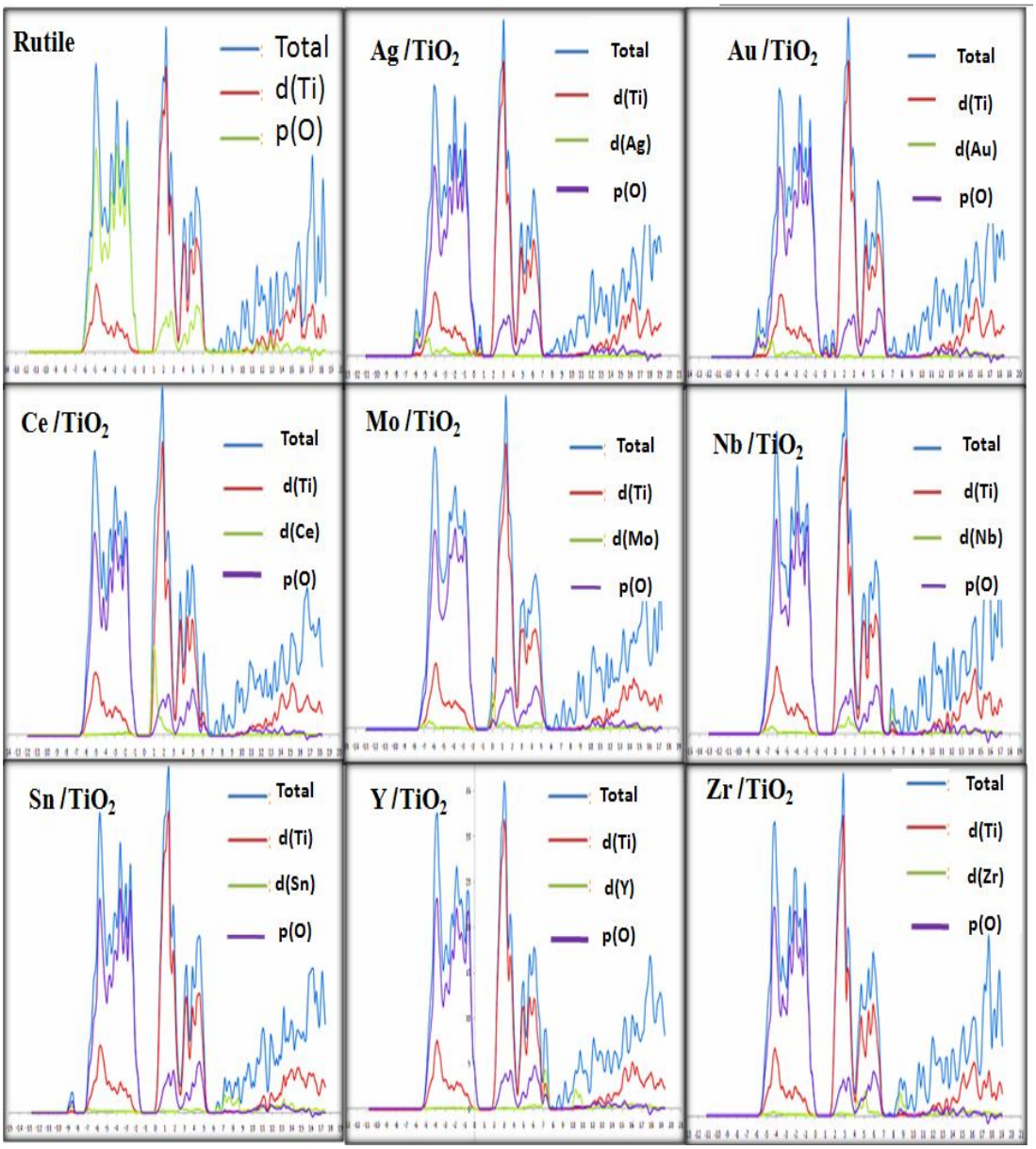

Fig. 4. The total and partial DOS of doped rutile TiO_2 compare with Pure TiO_2.

stable than r-TiO_2 by 1.65 eV for the 48-atom supercell, which is in line with the previous theoretical findings [56]. However, it has been reported that such a small stability limit, given the crystal growth conditions and presence of impurities, makes a-TiO_2 stabilization impossible, and thus phase transformation from a-TiO_2 to r-TiO_2 becomes irreversible [57].

Doped TiO_2

Impurity (Im) atoms have been connected to six adjacent O atoms, forming a body-centered octahedral for $Im_1Ti_{15}O_{32}$ systems. However, in $Im_1Ti_{15}O_{31}$ systems, they are connected to five O atoms. The cell parameters of anatase and rutile supercells have been calculated for all doped TiO_2. For pure TiO_2, the constants of the supercell, a,

and c are 7.564, and 9.564 Å in anatase, and 9.210, and 5.920 Å in rutile, respectively. On the other hand, these values change in $Im_1Ti_{15}O_{32}$ systems. As expected from the ionic radius, impurities can increase the cell volume in anatase and rutile phase. Table 1 indicates the parameters of pure and doped anatase and rutile cells.

To investigate the effect of impurities on relative stability of a-TiO_2 on r-TiO_2, the structural ground state energy of TiO_2 doped with different impurities was calculated in both a-TiO_2 and r-TiO_2 systems [58]. Table 2 compares the stability of anatase and rutile in response to cationic doping by Y, Zr, Nb, Mo, Ag, Sn, Au and Ce. Experimental studies [59] indicated that Ce dopant acts as an anatase phase stabilizer. Ionic radius of Ce^{3+} (1.14 Å) and Ce^{4+} (0.97 Å) was greater than the ionic radius of Ti^{4+} (0.61 Å), so, locating Ce^{3+}/ Ce^{4+} prefers bulk structures with more empty space between their atoms (prefers anatase *vs*. rutile). Therefore, it could be concluded that Ce as dopant should stabilize anatase more than rutile phase, and this is clearly found from relative stability of anatase vs. rutile data in Table 2. On the other hand, Sn^{4+} has more similar ionic radius (0.71 Å) and electronegativity (1.8) to Ti^{4+} and it is predicted that this cation has less relative stability of anatase vs. rutile. The data in Table 2 presents that relative stability of anatase *vs*. rutile for Sn^{4+} is 1.57 eV, which is even less than that of Ti^{4+}.

Cations with an ionic radius larger than titanium prevent anatase to rutile phase transformation [60-64]. In this regard, substitution of Ce and Zr impurities instead of Ti enhances relative stability of anatase to rutile, and prevents anatase to rutile transformation, which can in turn lead to enhanced photocatalytic performance of titania. However, other impurities reduce relative stability of anatase to rutile and accelerate anatase to rutile transformation, causing diminished photocatalytic performance of titania. Among cations, Ce and Zr with 0.4 and 0.12 eV respectively have the greatest impact on enhancing anatase to rutile relative stability. Au, Ag and Mo cations prefer rutile and reduce relative stability of anatase to rutile with energy of 0.62, 0.54 and 0.44 eV, respectively. Further, comparing the relative stability of phases in terms of atomic radius and ionic radius of impurities reveals that, as mentioned previously, atoms with nearly the same charge and larger than Ti are stable more in anatase compared to rutile phase. However, cations with low valence charges such as Au, Ag and Y, despite their large cationic radius destabilize the anatase phase.

Figure 3 displays the band structure and DOS of titania phases with different dopants. As the calculations revealed, Y, Nb and Mo significantly increased the gap in both phases in which Nb induced the highest growth among the dopants by 0.7 eV increase in anatase phase. Moreover, Ce and Au had the highest impact in reducing the gap of 0.07 eV in the anatase and Sn by 0.13 eV in the rutile phase. However, this impact is not large enough to cause a significant activity within the visible range. In addition, among the dopants, Au and Ag managed to create defect levels inside the gap which will result in photocatalytic activities in visible range.

The pDOS calculation analysis (Fig. 4) reveals that unlike the 3d elements that cause the defect states in the gap [65,66], in this study, with the exception of Ag and Mo, the energy of cations of 4d-orbitals is not large enough to appear inside the gap. Instead, they appear in the upper part of the conduction band. Like pure titanium of the edges of the conduction band and the valence band, they are composed of titanium d-orbitals and oxygen p-orbitals, respectively. By increasing the atomic number from Y to Mo during the row, 4d-orbital energy of the 4d elements moves towards lower energies, where d-levels of Mo appear below the conduction band. In the case of Y, the emergence of empty oxygen p-orbital levels above the valence band is due to a lower Y capacity than Ti (3+ and 4+, respectively), so it cannot provide enough electrons to fill the oxygen p-orbitals. The pDOS calculation analysis indicated that the overlap of Au and Ag d-orbitals with oxygen p-orbitals causes defect states inside the gap. Also, the Ce empty f-orbitals appear below and attached to the conduction band reducing the value of gap energy.

Doped-TiO_2 with O-vacancy

Oxygen vacancy causes expansion of pure and impure anatase and rutile structures. Previous studies have reported that a smaller dopant atom tends to pull in the surrounding O atoms, whereas a larger dopant atom tries to expel out coordinated O atoms [67].

Table 3 provides the parameters of pure and doped anatase and rutile bulk along with oxygen defect. The results reveal that development of oxygen defect has a slight

Table 1. Supercell Volume of Pure and Doped Anatase and Rutile TiO_2

System (structure)	Volume (anatase) $(Å)^3$	Volume (rutile) $(Å)^3$	%Volume change in anatase phase	%Volume change in rutile phase
PureTiO_2	5.75	5.25	0	0
Y/TiO_2	5.98	5.38	4	2.48
Zr/TiO_2	5.84	5.32	1.56	1.33
Nb/TiO_2	5.80	5.29	0.87	0.76
Mo/TiO_2	5.80	5.34	0.87	1.71
Ag/TiO_2	5.88	5.32	2.26	1.33
Sn/TiO_2	5.86	5.32	1.91	1.33
Au/TiO_2	5.88	5.33	2.26	1.52
Ce/TiO_2	5.99	5.40	2.43	2.86

Table 2. Comparing Anatase and Rutile Stability in Response to Cationic Doping. Atomic and Ionic Radius are Presented Too

Dopants	Ti	Y	Zr	Nb	Mo	Ag	Sn	Au	Ce
Relative anatase stability *vs* rutile (eV)	1.65	1.59	1.77	1.65	1.21	1.11	1.57	1.03	2.03
Atomic radius (Å)	1.45	1.81	1.60	1.43	1.36	1.44	1.41	1.44	1.14
Ionic radius (Å)	0.68	0.93	0.79	0.70	0.62	1.26	0.71	1.37	0.97
Capacity	+4	+3	+4	+5	+6	+1	+4	+1	+4

effect on the cell parameters of anatase structures doped with dopants, whereas this effect in rutile structures is considerable. Among all these structures, only in rutile structures with Mo, and Ce, doping plus oxygen defect has caused relative contraction. This behavior can be associated to altered oxidation state of Ti and dopant atom located close to the oxygen defect. With reduction of the oxidation state, the ionic radius and thus the cell volume increase. This effect is more evident in the rutile structure, for which the distance between atoms is smaller. The results of this research revealed that both doped atoms and their oxygen vacancy influence the cell volume of doped TiO_2 structure, such that these two effects cause increased percentage of cell volume enlargement for rutile compared to anatase [68,69].

Finally, as an important factor in titania activity, we examined the oxygen vacancy formation energy in the studied structures. The oxygen vacancy formation energies in pure and doped anatase and rutile structures were calculated by the following relation:

Table 3. Supercell Volume (in $Å^3$) of Pure and Doped Anatase and Rutile TiO_2 with Oxygen Deficiency

System (structure)	Supercell volume (anatase)	Supercell volume (rutile)	%Volume change (anatase)	%Volume change (rutile)
TiO_2 With O-vacancy	5.77	5.49	0	0
Y WithO-vacancy /TiO_2	5.95	5.93	3.11	8.01
Zr With O-vacancy /TiO_2	5.86	5.72	1.55	4.19
Nb With O-vacancy /TiO_2	5.80	5.60	0.52	2.00
Mo With O-vacancy /TiO_2	5.79	5.47	0.35	-0.36
Ag With O-vacancy /TiO_2	5.89	5.71	2.08	4.01
Sn With O-vacancy /TiO_2	5.93	5.56	2.77	1.27
Au With O-vacancy /TiO_2	5.87	5.87	1.73	6.92
Ce With O-vacancy /TiO_2	6.00	5.47	2.60	-0.36

Table 4. The Formation Energy (in eV) of Oxygen Vacancy in Pure and Doped a-TiO_2 and r-TiO_2 Structures

Dopant	Anatase	Rutile	ΔE (eV) = E(a-TiO_2) - E(r-TiO_2)
No Dopant	4.70	4.24	1.2025878
Y	2.40	1.41	0.330620553
Zr	4.99	4.24	1.02656511
Nb	5.05	4.87	1.476200581
Mo	4.62	4.81	1.399643616
Ag	0.13	-0.14	0.838874187
Sn	2.96	3.02	1.02618112
Au	0.90	0.70	0.825207698
Ce	4.93	2.576	-0.32066857

E_f = E(system with defect) - E (system without defect) + μ(O)

where E (system without defect) and E (system with defect) are the total energy of pure a-TiO_2 and r-TiO_2, and those with dopants for cases without and with oxygen vacancy, respectively. In comparative conditions, μ(O) oxygen chemical potential can be considered to be equal to half of the O_2 ground state energy [70,71].

Table 4 provides the oxygen vacancy formation energy

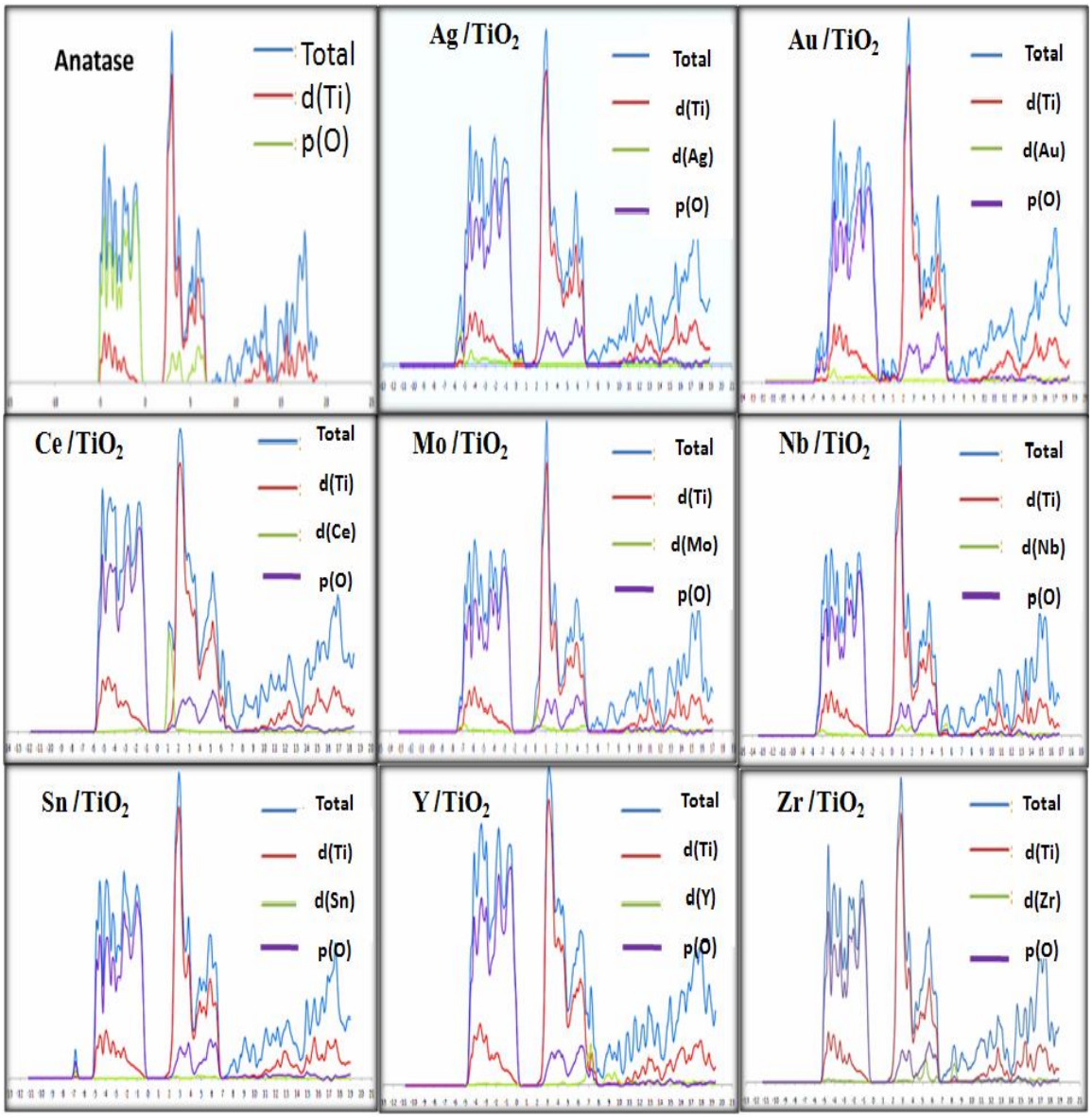

Fig. 5. The total and partial DOS of doped anatase TiO_2 compare with Pure TiO_2.

in pure and doped a-TiO_2 and r-TiO_2 structures. The results showed that the oxygen vacancy formation energy for a-TiO_2 and r-TiO_2 is 4.70 and 4.25 eV, respectively, which is in agreement with the previous calculations [72].

The results also indicated that almost all dopants reduce the energy required for formation of oxygen vacancy, which in turn can cause their enhanced performance. Meanwhile, Ag within the titania structure minimizes oxygen vacancy formation energy to -0.14 eV in rutile and 0.13 eV in anatase structure in comparison with other elements. Out of dopants, Y, Zr, Nb, Ag, Au, Ce, as with pure titania, enable development of defect in rutile phase with a lower energy compared to anatase. However, Sn and Mo cause accelerated development of defect in anatase compared to rutile (the lower defect formation energy in anatase in relation to rutile) which can enhance their performance in

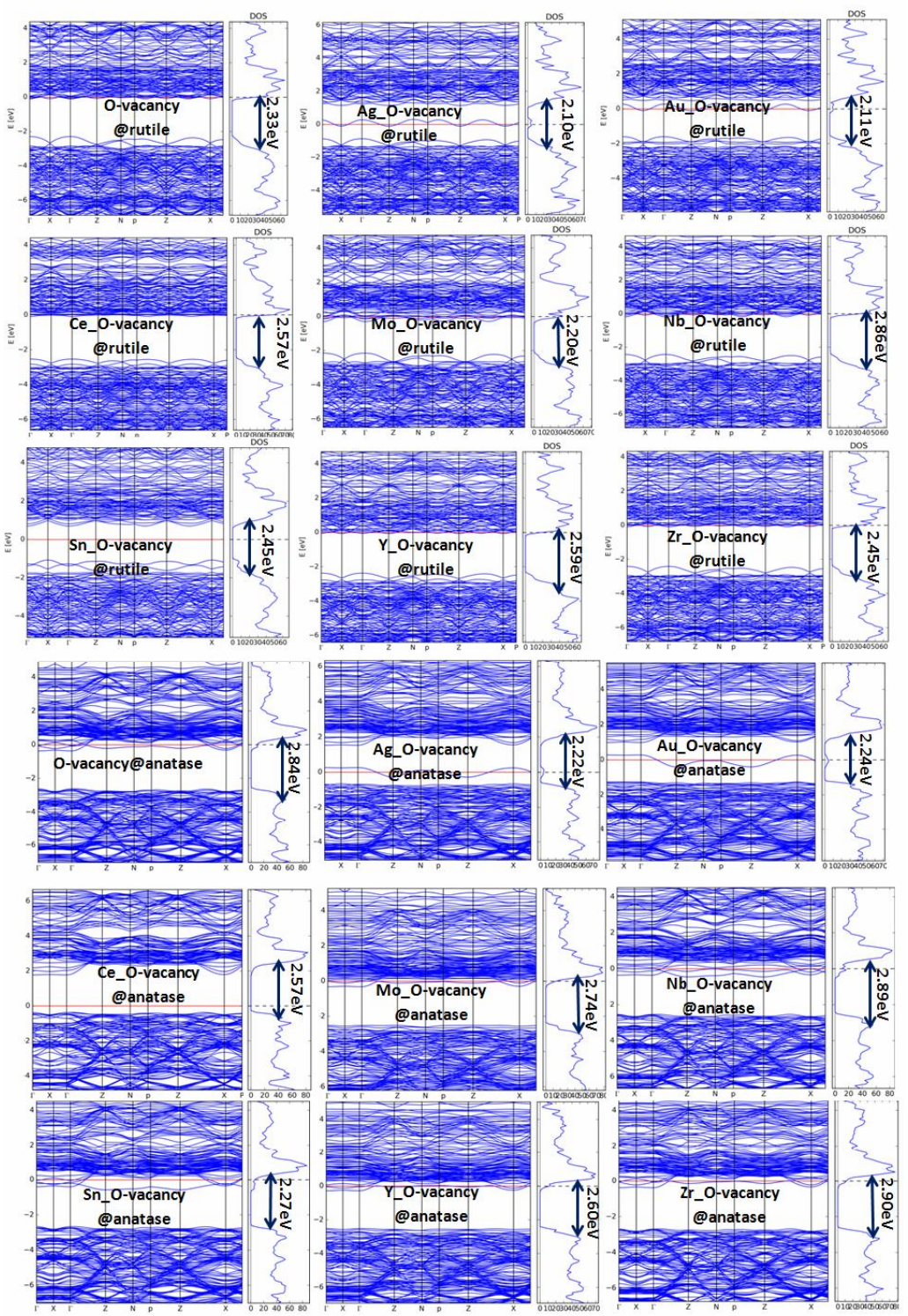

Fig. 6. The total DOS and band structure of doped anatase and rutile TiO_2 compare with Pure TiO_2 along with O-vacancy defect. Red solid line represents of the Fermi level. The band gap values were determined from Γ point, where the defect sates inside the gap were ignored.

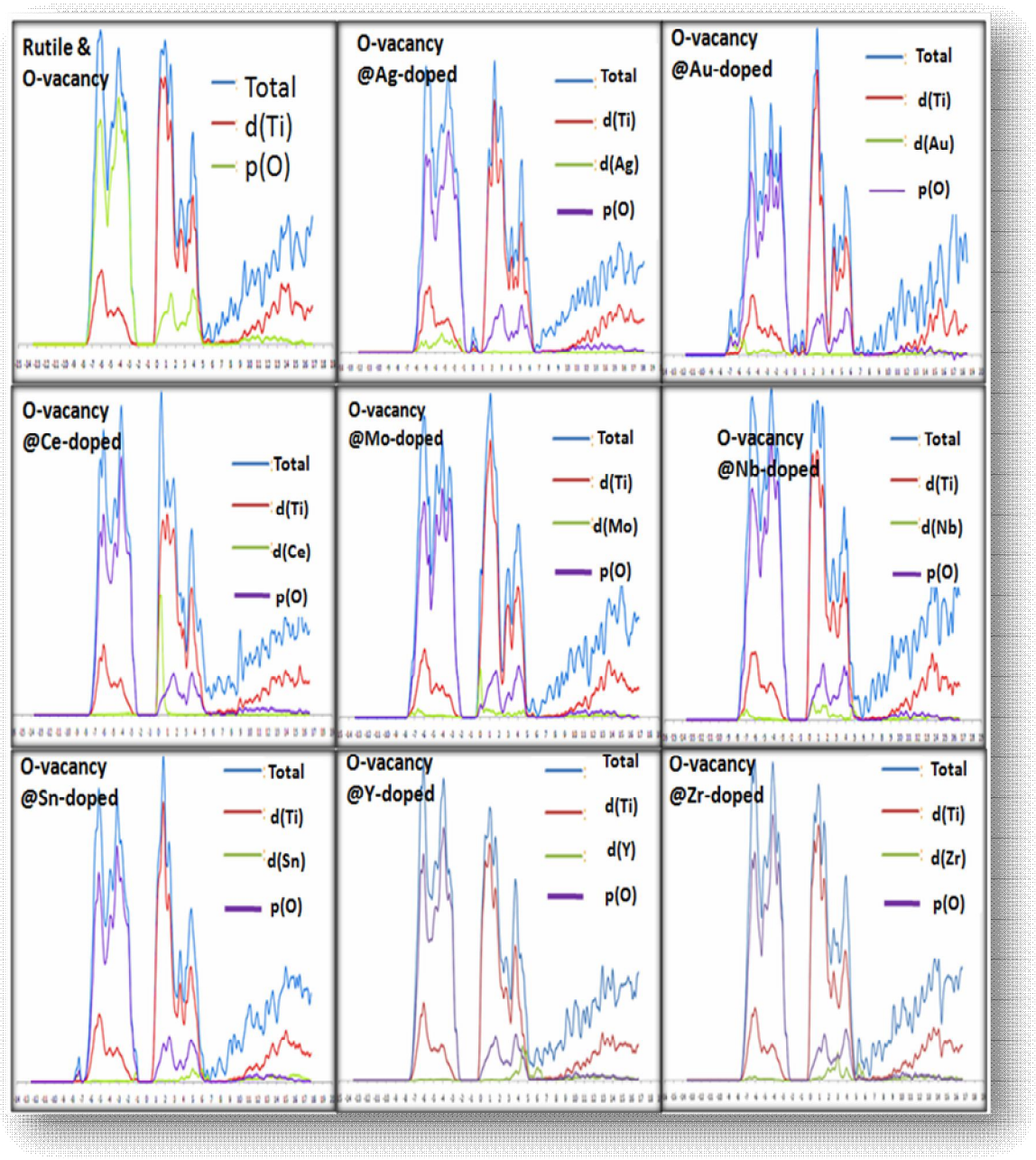

Fig. 7. The total and partial DOS of doped rutile TiO_2 compare with Pure TiO_2 along with O-vacancy defect.

photocatalytic processes. Moreover, Nb and Mo dopants along with oxygen defect prevent anatase to rutile transformation, where Nb and Mo cause increased relative stability of anatase to rutile by around 0.3 and 0.2 eV, respectively. The rest of elements alongside oxygen defect facilitate anatase to rutile transformation. XPS results confirm computations in this research, where formation of oxygen vacancy causes increased anatase to rutile phase transformation rate [73].

The results predict that Ce and Zr dopants in defect-free

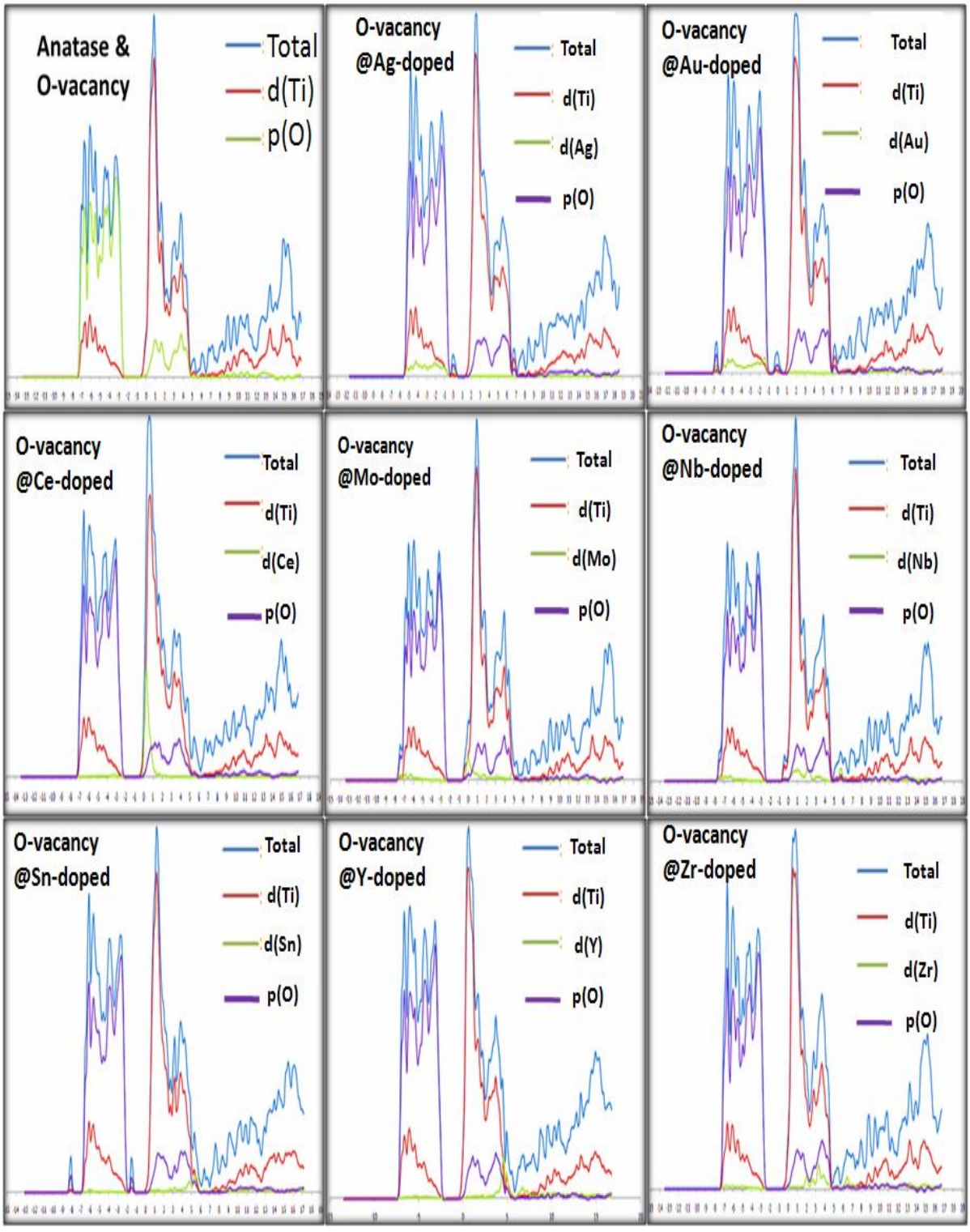

Fig. 8. The total and partial DOS of doped anatase TiO_2 compare with Pure TiO_2 along with O-vacancy defect.

titania crystals cause enhanced photocatalytic activity by elevating the relative stability of anatase. Nevertheless, Sn, Ce, Y, Au and Ag lead to a significant reduction in oxygen vacancy formation energy, which is an important factor in enhancing photocatalytic activity. Therefore, two important influential parameters in titania photocatalytic, *i.e.*, anatase to rutile phase transformation and development of oxygen vacancy, are highly dependent on synthesis conditions, which act in contrast to each other. This itself can be due to the incongruent experimental results in response to dopants in altering titania photocatalytic activity.

The analysis of electronic structures of doped and pure titania with oxygen vacancies showed that except for Ag, Au and Sn-doped titania, oxygen vacancy will create occupied defect levels below the conduction band as outlined in Fig. 5. This implies that the structures are n-type semiconductors. Among them, in both phases of Ag- and Sn-doped titania, the Fermi level was in the middle of gap. Similar to non-defected structures, Au and Ag created impurity levels in the middle of gap. As the last point, the oxygen vacancy significantly increased the gap.

The analysis of pDOS results (Fig. 6) shows that the titanium filled d-orbitals' proportion is below the conduction band due to the defect of O-vacancy, which results in n-type semiconductor. In the case of Au, Ag and Sn impurities, the overlapping of oxygen p-orbitals with Au and Ag d-orbitals and Sn s, p-orbitals causes defect states in the gap.

CONCLUSIONS

Theoretical investigations based on density functional theory were performed using a full potential method on pure anatase and rutile structures (titania) and with Y, Zr, Nb, Mo, Ag, Sn, Au, Ce dopants, which replaced Ti atom in the structure. The results suggested that Ce and Zr, with crystalline structure without defect prevent anatase to rutile transformation, and cause enhanced titania photocatalytic activity. However, doping titania with other cations under conditions of crystalline structure without defect facilitates anatase to rutile transformation, causing diminished photocatalytic active phase of anatase in the general composition. Further, oxygen vacancy formation calculations were performed in pure and doped anatase and rutile. It was found that presence of dopant significantly reduces the oxygen defect formation energy, among which Sn, Ce, Au, Ag and Y have the greatest impact in energy reduction. In addition, Sn and Mo caused accelerated defect development in anatase compared to rutile. The studies also revealed that for atoms with the same valence and larger than Ti, atomic radius are a very suitable parameter to predict anatase to rutile transformation rate and cations with low valence charges such as Au, Ag, and Y, despite their large cationic radius, destabilize the anatase phase. For all of the studied elements with a valence less than that of Ti, presence of dopant accelerates the transformation. The electronic structure of doped titania showed that none of the impurities can make a significant reduction in anatase and rutile phases. Moreover, Ag and Au can activate the photocatalytic properties in visible range by creating defect levels inside the gap. Presence of oxygen vacancies significantly increased the band gap energy for all the samples. In most of the cases, formation of occupied defect levels below the conduction band resulted in creation of n-type semiconductor.

REFERENCES

[1] Farahmandjou, M., Fabrication and characterization of rutile TiO_2 nanocrystals by water soluble precursor, *Phys. Chem. Res.* **2015**, *3*, 293-298, DOI: 10.22036/pcr.2015.10641.

[2] kimiagar, S., Hydrophilicity and antibacterial properties of Ag/TiO_2 nanoparticle, *Phys. Chem. Res.* **2013**, *1*, 126-133, August, DOI: 10.22036/pcr.2013.3223.

[3] Elahifard, M. R.; Rahimnejad, S.; Haghighi, S.; Gholami, M. R., Apatite-coated Ag/AgBr/TiO_2 visible-light photocatalyst for destruction of bacteria, *J. Am. Chem. Soc,* **2007**, *129*, 9552-9553, DOI: 10.1021/ja072492m.

[4] Azimzadehirani, M.; Elahifard, M. R.; Haghighi, S.; Gholami, M. R., Highly efficient hydroxyapatite/TiO2 composites covered by silver halides as E. coli disinfectant under visible light and dark media, *J. Photochem. Photobiol. Sci.* **2013**, *12*, 1787-1794, DOI: 10.1039/c3pp50119a.

[5] Padervand, M.; Salari, H.; Ahmadvand, S.; Gholami, M. R., Removal of an organic pollutant from waste

water by photocatalytic behavior of AgX/TiO_2 loaded on mordenite nanocrystals, *Res. Chem. Intermed.* **2012**, *38*, 1975-1985, DOI 10.1007/s11164-012-0519-8.

[6] Elahifard, M. R.; Padervand, M.; Yasini, S.; Fazeli, E., The effect of double impurity cluster of Ni and Co in TiO_2 bulk; a DFT study, *J. Electroceram.* **2016**, *37*, 4536-4544, DOI: 10.1007/s10832-016-0027-0.

[7] Elahifarda, M.R.; Vatan Meidanshahib, R., Photo-deposition of Ag metal particles on Ni-doped TiO_2 for photocatalytic application, *Prog. React. Kinet. Mech.* **2017**, *42*, 244-250, DOI: 10.3184/146867817x14821527549130.

[8] Elahifard, M. R.; Gholami, M. R., Acid blue 92 photocatalytic degradation in the presence of scavengers by two types photocatalyst, *Environ. Prog. Sus. Energy.* **2012**, *31*, 371-378, DOI: 10.1002/ep.10558.

[9] Padmanabhan, S. C. S.; Pillai, C.; Colreavy, J.; Balakrishnan, S.; McCormack, D. E.; Perova, T. S.; Hinder, S. J.; Kelly, J. M., A simple sol-gel processing for the development of high-temperature stable photoactive anatase titania, *J. Chem. Mater.* **2007**, *19*, 4474-4481, DOI: 10.1021/cm070980n .

[10] Mohammadrezaei, V.; Ebrahimi, M.; Beyramabadi, S. A., Study of the effect of molecular cluster size alanine concentrations in water by using the activity coefficient method and density functional theory, BULG CHEM COMMUN, 2017, Special Issue J., 147-151.

[11] Madaeni, S. S.; Ghaemi, N., Characterization of self-cleaning RO membranes coated with TiO_2 particles under UV irradiation, *J. Membrane. Sci.* **2007**, 303, 221-233, DOI: 10.1016/j.memsci.2007.07.017 .

[12] Zhang, A.; Yan-Ping, S., Photocatalytic killing effect of TiO_2 nanoparticles on Ls-174-t human colon carcinoma cells, *World J. Gastroenterology.* **2004**, *10*, 3191-3193, DOI: 10.3748/wjg.v10.i21.3191 .

[13] Biju, P.; Mahaveer, K., Effect of crystallization on humidity sensing properties of sol-gel derived nanocrystalline TiO_2 thin films, *J. Solid Films.* **2008**, *516*, 2175-2180, DOI: 10.1016/j.tsf.2007.06.147.

[14] Ahmadvand, S.; Zaari, R.; Varganov, S. A., Spin-forbidden and spin-allowed cyclopropenone (c-H_2C_3O) formation in interstellar medium, *Astrophys. J.* **2014**, *795*, 173-177, DOI: 10.1088/0004-637X/795/2/173.

[15] Mahshid, S.; Askari, M.; Sasani-Ghamsari, M., Synthesis of TiO_2 nanoparticles by hydrolysis and peptization of titanium isopropoxide solution, *J. Phys. Quantum. Elec. Optoelec.* **2006**, *9*, 658-663, DOI: 10.1016/j.jmatprotec.2007.01.040 .

[16] Choi, W.; Andreas, T.; Hoffmann, R. M., The role of metal ion dopants in quantum-sized TiO_2: correlation between photoreactivity and charge carrier recombination dynamics, *J. Phys. Chem.* **1994**, *98*, 13669-13679, DOI: 10.1021/j100102a038 .

[17] Pillai, S.; Pillai, S. C.; Periyat, P.; George, R.; McCormack, D. E.; Seery, M. K.; Hayden, H.; Colreavy, J.; Corr, D.; Hinder, S. J., Synthesis of high-temperature stable anatase TiO_2 photocatalyst, *J. Phys. Chem. C.* **2007**, *111*, 1605-1611, DOI: 10.1021/jp065933h.

[18] Poulsen, E.; James, A., Extractive metallurgy of titanium: a review of the state of the art and evolving production techniques, *JOM.* **1983**, *35*, 60-65, DOI: 10.1007/bf03338304.

[19] Enache, C. S., Characterization of Thin Film Photoanodes for Solar Water Splitting, University of Transilvania, PhD Thesis 2012, DOI: 10.1016/s0167-5729(02)00100-0.

[20] Kudo, A.; Yugo, M., Heterogeneous photocatalyst materials for water splitting, *J. Chem. Soc. Rev.* **2009**, *38*, 253-278, DOI: 10.1039/b800489g.

[21] Fujishima, A.; Rao, T. N.; Tryk, D. A., Titanium dioxide photocatalysis, *J. Photochem. Photobiol. Rev.* **2000**, *1*, 1-21, DOI: 10.1016/s1389-5567(00)00002-2.

[22] Linsebigler, A. L.; Lu, G.; Yates, J. T., Photocatalysis on TiO_2 surfaces: principles, mechanisms, and selected results, *J. Chem. Rev.* 1995, *95*, 735-758, DOI: 10.1021/cr00035a013 .

[23] Abe, R., Recent progress on photocatalytic and photoelectrochemical water splitting under visible light irradiation, *J. Photochem. Photobiol. C.* **2010**, *11*, 179-209, DOI: 10.1016/j.jphotochemrev.2011.02.003.

[24] Chen, X.; Mao, S. S., Synthesis, titanium dioxide nanomaterials: Synthesis, properties, modifications,

and applications, *J. Chem. Inform.* **2007**, *107*, 2891-2959, DOI: 10.1021/cr0500535.

[25] Kamat, P. V.; Flumiani, M.; Dawson, A., Metal-metal and metal-semiconductor composite nanoclusters, colloid. *Surf. Physicochem. Eng. Aspects.* **2002**, *202*, 269-279, DOI: 10.1016/s0927-7757(01)01071-8.

[26] Ni, M.; Leung, M. K. H.; Leung, D. Y. C.; Sumathy, K., A review and recent developments in photocatalytic water-splitting using TiO_2 for hydrogen production, *Rene. Sus. En. Rev.* **2007**, *11*, 401-425, DOI: 10.1016/j.rser.2005.01.009.

[27] Hameed, A.; Gondal, M. A.; Yamani, Z. H., Effect of transition metal doping on photocatalytic activity of WO_3 for water splitting under laser illumination: Role of 3d-orbitals, *J. Catal.* **2004**, *5*, 715-719, DOI: 10.1016/j.catcom.2004.09.002.

[28] Linsebigler, L., Photocatalysis on TiO_2 surfaces: principles, mechanisms, and selected results, *J. Chem. Rev.* **1995**, *95*, 735-758, DOI: 10.1021/cr00035a013.

[29] Wu, N. L.; Lee, M. S., Enhanced TiO_2 photocatalysis by Cu in hydrogen production from aqueous methanol solution, *Int. J. Hydr. En.* **2004**, *29*, 1601-1605, DOI: 10.1016/j.ijhydene.2004.02.013.

[30] Chen, W.; Yuan, P.; Zhang, S.; Sun, Q.; Liang, E.; Jia, Y., Electronic properties of anatase TiO_2 doped by lanthanides: A DFT + U study, *J. Physica. B: Condensed Matter.* **2012**, *407*, 1038-1043.

[31] Guo, M.; Du, J., First-principles study of electronic structures and optical properties of Cu, Ag and Au-doped anatase TiO_2, *J. Physica. B: Condensed Matter.* **2012**, *407*, 1003-1007, DOI: 10.1016/j.physb.2011.12.128.

[32] Guo, M. L.; Zhang, X. D.; Liang, C. T., Concentration-dependent electronic structure and optical absorption properties of B-doped anatase TiO_2, *J. Physica. B: Condensed Matter.* **2011**, *406*, 3354-3358, DOI: 10.1016/j.physb.2011.05.061.

[33] Rodríguez Torres, C. E.; Cabrera, A. F.; Fernández van Raap, M. B.; Sánchez, F. H., Study of mechanical alloyed Fe-doped TiO_2 compounds, *J. Physica. B: Condensed Matter.* **2004**, *354*, 67-70, DOI: 10.1016/j.physb.2008.11.032.

[34] Zhang, K. C.; Li, Y. F.; Liu, Y.; Zhu, Y., Possible ferromagnetism in Cd-doped TiO_2: A first-principles study, *J. Physica. B: Condensed Matter.* **2013**, *422*, 28-32, DOI: 10.1016/j.physb.2013.04.036.

[35] Cabrera, A. F.; Rodríguez Torres, C. E.; Errico, L.; Sánchez, F. H., Study of Fe-doped rutile TiO_2 alloys obtained by mechanical alloying, *J. Physica. B: Condensed Matter.* **2006**, *384*, 345-347, DOI: 10.1016/j.physb.2006.06.040.

[36] Ranki, V.; Saarinen, K., Formation of vacancy-impurity complexes in highly As- and P-doped Si, *J. Physica. B: Condensed Matter.* **2003**, *340*, 765-768, DOI: 10.1016/j.physb.2003.09.117.

[37] Almquist, B.; Pratim, B., Role of synthesis method and particle size of nanostructured TiO_2 on its photoactivity, *J. Catal.* **2002**, *212*, 145-156, DOI: 10.1006/jcat.2002.3783.

[38] Serpone, N., Is the band gap of pristine TiO_2 narrowed by anion- and cation-doping of titanium dioxide in second-generation photocatalysts?, *J. Phys. Chem. B.* **2006**, *110*, 24287-24293, DOI: 10.1021/jp065659r.

[39] Ranjit, K. T.; Cohen, H.; Willner, I.; Bossmann, S.; Braun, A. M., Lanthanide oxide-doped titanium dioxide: Effective photocatalysts for the degradation of organic pollutants, *J. Mater. Sci.* **1999**, *34*, 5273-5280, DOI: 10.1023/a:1004780401030.

[40] Nagaveni, K.; Hegde, M. S.; Ravishankar, N.; Subbanna, G. N.; Madrass, G., Synthesis and structure of nanocrystallineTiO2 with lower band gap showing high photocatalytic activity, *J. Langmuir.* **2004**, *20*, 2900-2907, DOI: 10.1021/la035777v.

[41] Chen, W.; Samuel, S., Titanium dioxide nanomaterials: synthesis, properties, modifications, and applications, *J. Chem. Rev.* **2007**, *107*, 2891-2959, DOI: 10.1021/cr0500535.

[42] Hongfei, L.; Yuzheng, G.; Robertson, J., Calculation of TiO_2 surface and subsurface oxygen vacancy by the screened exchange functional, *J. Phys. Chem. C.* **2015**, *119*, 18160-18166, DOI: 10.1021/acs.jpcc.5b02430.

[43] Dorian, A.; Hanaor, H.; Charles, C., Review of the anatase to rutile phase transformation, *J. Mater* Sci. **2011**, *46*, 855-874, DOI: 10.1007/s10853-010-5113-0.

[44] Heald, E. F.; Weiss, C. W., Kinetics and mechanism of the anatase/rutile transformation, as catalyzed by

ferric oxide and reducing conditions, *Am. Miner.* **1972**, *57*, 10-23, DOI: 10.1007/bf02065589.

[45] Janes, R.; Knightley, L. J.; Harding, C. J., Structural and spectroscopic studies of iron(III) doped titania powders prepared by sol-gel synthesis and hydrothermal processing, *J. Dyes Pig*. **2004**, *62*, 199-212, DOI: 10.1016/j.dyepig.2003.12.003.

[46] Gennari, F. C.; Pasquevich, D. M., Kinetics of the anatase-rutile transformation in TiO_2 in the presence of Fe_2O_3, *J. Mater. Sci.* **1998**, *33*, 1571-1578, DOI: 10.1023/a:1017515804370.

[47] Borkar, S. A.; Dharwadkar, S. R., Temperatures and kinetics of anatase to rutile transformation in doped TiO_2 heated in microwave field , *J. Therm. Anal. Calorim*. **2004**, *78*, 761-767, DOI: 10.1007/s10973-005-0443-0.

[48] Francisco, M. S.; Mastelaro, V. R., Inhibition of the anatase-rutile phase transformation with addition of CeO_2 to CuO-TiO_2 system: Raman spectroscopy, X-ray diffraction, and textural studies, *J. Chem. Mater.* **2002**, *14*, 2514-2518, DOI: 10.1021/cm011520b.

[49] Sun, C. Q., Study of electric quadrupole perturbation at multiple probe sites in Hf- doped rutile in a single perturbed angular correlation measurement, *J. Chem. Phys.* **2014**, *108*, 805-817, DOI: 10.1103/physrevb.1.1995.

[50] Pan, X. Y.; Yang, M. Q.; Fu, X. Z.; Zhang, N.; Xu, Y. J., Defective TiO_2 with oxygen vacancies: synthesis, properties and photocatalytic applications, *J. Nanoscale.* **2013**, *9*, 3601-3614, DOI: 10.1039/c3nr00476g.

[51] Blum, V.; Gehrke, R.; Hanke, F.; Havu, P.; Havu, V.; Ren, X.; Reuter, K.; Scheffler, M., *Ab initio* molecular simulations with numeric atom-centered orbitals, *Comput. Phys. Commun.* **2009**, *180*, 2175-2196, DOI: 10.1016/j.cpc.2009.06.022.

[52] Perdew, J.; Burke, K.; Ernzerhof, M., Generalized gradient approximation made simple, *J. Phys. Rev. Lett.* **1996**, *77*, 3865-3868, DOI: 10.1103/physrevlett.77.3865.

[53] Lenthe, E. V.; Snijders, J.; Baerends, E., The zero order regular approximation for relativistic effects: The effect of spin-orbit coupling in closed shell molecules, *J. Chem. Phys.* **1996**, *105*, 6505-6516, DOI: 10.1063/1.472460.

[54] Segall, M. D.; Shah, R.; Pickard, C. J., Population analysis of plane-wave electronic structure calculations of bulk materials, *J. Phys. Rev. B.* **1996**, *54*, 16317-16320, DOI: 10.1103/physrevb.54.16317.

[55] Cromer, D. T.; Herrington, K., The structures of anatase and rutile. *J. Am. Chem. Soc.* **1955**, *77*, 4708-4709, DOI: 10.1021/ja01623a004.

[56] Curtiss, L. A.; Carpenter, J. E.; Raghavachari, K., Pople JA Validity of additively approximations in Gaussian theory, *J. Chem. Phys.* **1992**, *96*, 9030-9034, DOI: 10.1063/1.462261.

[57] Dorian, A.; Hanaor, H.; Mohammed, H.; Assadi, N.; Sean, Li.; Aibing, Yu.; Charles, C., *Ab initio* study of phase stability in doped TiO_2, *J. Comput. Mech.* **2012**, *50*, 185-194, DOI: 10.1007/s00466-012-0728-4.

[58] Na-Phattalung, S.; Smith, M. F.; Kim, K.; Du, M. H.; Wei, S. H.; Zhang, S.; Limpijumnong, B., First-principles study of native defects in anatase TiO_2, *J. Phys. Rev.* **2006**, *73*, 125205-125211, DOI: 10.1103/physrevb.73.125205.

[59] Yang, J.; Fereira, J. M. F., On the titania phase transition by zirconia additive in a sol-gel-derived powder, *Mater. Res. Bull.* **1998**, *33*, 389-394, DOI: 10.1016/s0025-5408(97)00249-3.

[60] Shi, Z.; Yan, M. L.; Jin, L. N.; Lu, X. M.; Zhao, G., The phase transformation behaviors of Sn^{2+}-doped Titania gels, *J. Non-Cryst. Solids.* **2007**, *353*, 2171-2178, DOI: 10.1016/j.jnoncrysol.2007.02.048.

[61] Phillips, J. C., Ionicity of the chemical bond in crystals, *Rev. Mod. Phys.* **1970**, *42*, 317-356, DOI: 10.1103/revmodphys.42.317.

[62] Kumar, K. N.; Fray, D. J.; Nair, J.; Mizukami, F.; Okubu, T., Enhanced anatase-to-rutile phase transformation without exaggerated particle growth in nanostructured titania-tin oxide composites, *J. Scripta. Mater.* **2007**, *57*, 771-774, DOI: 10.1016/j.scriptamat.2007.06.039.

[63] Smith, S. J.; Stevens, R.; Liu, S.; Li, G.; Navrotsky, A.; Boerio-Goates, J.; Woodfield, B. F., Heat capacities and thermodynamic functions of TiO_2 anatase and rutile: analysis of phase stability. *Am. Mineral.* **2009**, *94*, 236-243, DOI: 10.2138/am.2009.3050.

[64] Zhang, H.; Banfield, J. F., Thermodynamic analysis of phase stability of nanocrystalline titania. *J. Mater. Chem.* **1998**, *8*, 2073-2076, DOI: 10.1039/a802619j.

[65] Du, X. S.; Li, Q. X.; Su, H. B.; Yang, J. L., Electronic and magnetic properties of V-doped anatase TiO_2 from first principles, *J. Phys. Rev. B.* **2006**, *74*, 233201-233204, DOI: 10.1103/physrevb.74.233201.

[66] Wang, Y. Q.; Zhang, R. R.; Li, J. B.; Li, L. L.; Lin, S. W., First-principles study on transition metal-doped anatase TiO2, *Nanoscale. Res. Lett.* **2014**, *9*, 46-53, DOI: 10.1186/1556-276x-9-46.

[67] Shannon, R. D.; Pask, J. A., Kinetics of the anatasr-rutile transformation, *J. Am. Ceram. Soc.* **1965**, *48*, 391-398, DOI: 10.1111/j.1151-2916.1965.tb14774.x.

[68] Koshitani, N.; Sakulkhaemaruethai, S.; Suzuki, Y.; Yoshikawa, S., Preparation of mesoporous titania nanocrystals using alkylamine surfactant templates, *J. Ceram. Inter,* **2006**, *32*, 829-824, DOI: 10.1016/j.ceramint.2005.06.009.

[69] Hao, W. C.; Zheng, S. K.; Wang, C.; Wang, T. M., Comparison of the photocatalytic activity of TiO_2 powder with different particle size, *J. Mater. Sci. lett.* **2002**, *21*, 1627-1629, DOI: 10.1023/a:1020386019893.

[70] Zhao, Y. F.; Song, C. Li.; Jin, Lu. Li.; Yan, Y. Y.; Leng, G.; Xin, Y. N.; Liu, J., Effects of oxygen vacancy on 3d transition-metal doped anatase TiO_2: First principles calculations, *Chem. Phys. Lett.* **2016**, *36*, 647-669, DOI: 10.1016/j.cplett.2016.01.040.

[71] VandeWalle, C. G.; Neugebauer, J., First-principles calculations for defects and impurities: applications to III-nitrides, *J. Appl. Phys.* **2004**, *95*, 3851-3879. DOI: 10.1063/1.1682673.

[72] Li, X. Z.; Li, F. B., Study of Au/Au^{3+}-TiO_2 photocatalysts toward visible photooxidation for water and wastewater treatment, *J. Environ. Sci. Tech.* **2001**, *35*, 2381-2387, DOI: 10.1021/es001752w.

[73] Cao, Y.; Yang, W.; Zhang, W. Liub, G.; Yue, P., Improved photocatalytic activity of Sn^{4+} doped TiO_2 nanoparticulate films prepared by plasma-enhanced chemical vapor deposition, *J. Chem.* **2004**, *28*, 218-222, DOI: 10.1039/b306845e.